

Probing Dark Matter Substructure with Pulsar Timing

E. R. Siegel,^{1,2*} M. P. Hertzberg³ and J. N. Fry²

¹*Department of Physics, University of Wisconsin, Madison, WI, 53706, USA*

²*Department of Physics, University of Florida, Gainesville, FL, 32611-8440, USA*

³*Center for Theoretical Physics, Massachusetts Institute of Technology, Cambridge, MA, 02139, USA*

Accepted ??? ?????. Received ??? ?????. in original form 2007 February 19

ABSTRACT

We demonstrate that pulsar timing measurements may potentially be able to detect the presence of dark matter substructure within our own galaxy. As dark matter substructure transits near the line-of-sight between a pulsar and an observer, the change in the gravitational field will result in a delay of the light-travel-time of photons. We calculate the effect of this delay due to transiting dark matter substructure and find that the effect on pulsar timing ought to be observable over decadal timescales for a wide range of substructure masses and density profiles. We find that transiting dark matter substructure with masses above $10^{-2} M_{\odot}$ ought to be detectable at present by these means. With improved measurements, this method may be able to distinguish between baryonic, thermal non-baryonic, and non-thermal non-baryonic types of dark matter. Additionally, information about structure formation on small scales and the density profiles of galactic dark matter substructure can be extracted via this method.

Key words: gravitation, pulsars: general, Galaxy: halo, dark matter, large scale structure of Universe

1 INTRODUCTION

One of the most fundamental goals of cosmology is to determine the composition of the universe. Contrary to our experience in the solar system, where the emitted light traces the mass distribution, the vast majority of matter in the universe appears to be non-luminous. This puzzle is known as the dark matter problem. One of the greatest goals in modern cosmology is to determine the nature and properties of this dark matter. Although many solutions have been proposed explaining the presence of dark matter, its nature remains mysterious, as all but the most indirect methods of detection have been unsuccessful thus far.

The astrophysical evidence for the existence of dark matter is overwhelming, as recently reviewed in Siegel et al. (2006). While the amount of matter in luminous sources is only $\Omega_{*} \simeq 0.005$ (Fukugita & Peebles 2004; Shankar et al. 2006), precision measurements of the cosmic microwave background (Spergel et al. 2006) and type Ia supernovae (Riess et al. 2006) indicate that the total amount of matter is $\Omega_m \simeq 0.26$, or that 98 per cent of the matter in the universe is non-luminous. While a significant component of this non-luminous matter can be baryonic, nucleosynthesis (Fields & Olive 2006), Silk damping effects (Miller, Nichol, & Chen 2002), and searches for MASSive Compact Halo Objects (MACHOs) (Alcock et al. 1998) con-

strain the amount of baryonic matter to be $\Omega_b \approx 0.04$. This means that, although a portion of the dark matter is baryonic (~ 13 percent), the vast majority of matter in the universe is both non-luminous and non-baryonic (Ω_{DM}). This non-baryonic dark matter must also be cold; i.e., it must have become non-relativistic at early times, as evidenced most clearly by the large amount of power on small scales at early times in the Lyman- α forest (Viel et al. 2005). This constraint eliminates the only standard-model candidate for non-baryonic dark matter, the neutrino. There are then two generic classes of candidates for cold, non-baryonic dark matter: the thermal relic and the non-thermal relic. A thermal relic is a particle produced by thermally efficient interactions in the background plasma of the early universe. Its abundance then freezes out as the temperature drops, but it remains in kinetic equilibrium with the background plasma until later times (Bertschinger 2006). Examples of thermal relic dark matter candidates include the lightest supersymmetric particle, lightest Kaluza-Klein particle, and other particles generically classified as Weakly Interacting Massive Particles (WIMPs). On the other hand, non-thermal relics can be produced at phase transitions by vacuum misalignment mechanisms, and are born non-relativistic. Examples of non-thermal dark matter candidates include axions (Peccei & Quinn 1977; Weinberg 1978; Wilczek 1978) and massive gravitons (Dubovsky, Tinyakov, & Tkachev 2005). Finally, it is possible that both thermal and non-thermal

* E-mail: esiegel2@wisc.edu

types of dark matter exist, and that Ω_{DM} is made up of a composite of these two classes.

In a recent and exciting development, non-baryonic dark matter has been detected indirectly via its gravitational influence in the Bullet Cluster (Clowe et al. 2006). Since baryons, thermal relic dark matter, and non-thermal dark matter all decouple from the primordial plasma at different times and possess different interactions, it is expected that the small-scale structure that forms composed of these types of matter will be quite different from one another. Baryons will remain in either diffuse gas clouds or collapse to form MACHOs, thermal dark matter will have its small scale structure on scales below 10^{-4} to $10^{-6} M_{\odot}$ suppressed by Silk damping, whereas non-thermally produced dark matter will have no such cutoff in its spectrum. Thermal dark matter will produce, on small scales, diffuse WIMP microhalos after gravitational collapse down to masses of about one Earth mass (Green, Hofmann, & Schwarz 2005; Loeb & Zaldarriaga 2005; Diemand, Moore, & Stadel 2005; Bertschinger 2006), whereas non-thermal dark matter will produce collapsed structure down to much smaller mass scales, without a cutoff in the spectrum, which will produce Non-thermal Axionic Collapsed HalOS (NACHOs). Under certain circumstances (Sikivie 2006; Zurek, Hogan, & Quinn 2006), the non-thermal dark matter will produce halos with substantial enhancements in density and abundance at $\sim 10^{-12} M_{\odot}$, known as axion miniclusters. In either case, these dark matter structures on the smallest scales may survive intact to the present day as substructure within larger collapsed structure such as our own galaxy (Goerdt et al. 2006). While large-scale dark matter structures like our galaxy’s halo are expected to be smooth to a simple approximation, realistic models include clumps, cusps, and possibly caustics.

This paper demonstrates that pulsar timing measurements can be used to probe the dark matter substructure in our own galaxy which transits across the line-of-sight between a pulsar and an observer. As the dark matter substructure transits, the variation in the light-travel-time of the pulses is of sufficient magnitude that the more stable millisecond pulsars should be able to not only detect the substructure, but to discriminate between the different signatures of MACHOs, NACHOs, and WIMPs. The remainder of this paper is laid out as follows. Section 2 presents a derivation of the delay in the light-travel-time due to a gravitational source intervening near or across the line-of-sight between an emitter and an observer, providing a number of examples. Section 3 applies this idea to the physical case of using pulsar timing measurements to detect the intervening dark matter substructure between Earth and the pulsar of interest. Section 4 discusses the possibility of differentiating between different types of dark matter and constraining its properties through precision timing measurements. Finally, Section 5 summarizes the major successes and drawbacks of this method, detailing the challenges of using pulsar timing to search for dark matter in our own galaxy.

2 GRAVITATIONAL TIME DELAY

One consequence of general relativity is the delay in the light-travel-time (l.t.t.) due to intervening gravitational

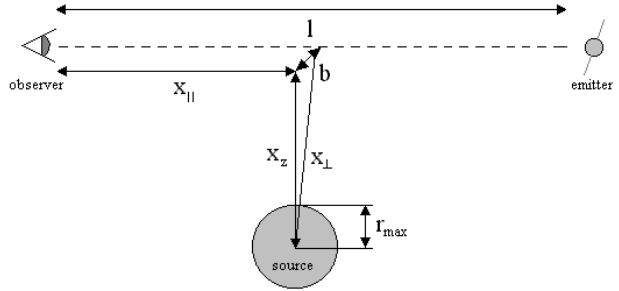


Figure 1. The generic configuration for a fixed emitter and observer, with a gravitational source of radius r_{max} transiting across or close to the line-of-sight. The emitter-observer distance is taken to be l , while the gravitational source has a distance to the observer \vec{x} and a velocity \vec{v} , both of which have components perpendicular (x_{\perp} , v_{\perp}) and parallel (x_{\parallel} , v_{\parallel}) to the line-of-sight. The minimum distance between the gravitational source and the line-of-sight as the source transits is defined as the impact parameter, b .

sources between an emitter and an observer (Shapiro 1964). This effect, known (for a point source) as the Shapiro time delay, is one of the classic solar system tests of Einstein’s relativity (Baez & Bunn 2005). This effect can be applied to extended sources and larger scales as well. If any collapsed substructure within our galaxy transits across the line-of-sight (l.o.s.) between an emitter and an observer, then the l.t.t. will be altered by the gravitational presence of the galactic substructure. The remainder of this Section is devoted to a derivation of the magnitude of the delay in the l.t.t. due to transiting collapsed substructure.

Consider the configuration shown in Figure 1: an emitting source is a fixed distance l from an observer, with a transiting gravitational source near the l.o.s., with a minimum distance to the l.o.s. (i.e. impact parameter) b . The gravitational source has a velocity $\vec{v}(t)$ and position $\vec{x}(t)$, where the velocity, assumed to be constant, has components parallel (v_{\parallel}) and perpendicular (v_{\perp}) to the l.o.s., while the position deviates from its initial value only in the direction given by \vec{v} . The two cases of physical importance to consider are when the radial size of the gravitational source (r_{max}) is either greater or smaller than the impact parameter, b .

To determine the time delay induced by the presence of this gravitational source, we integrate a null geodesic from the emitter to the observer. We consider the weak-field metric for a single gravitational source,

$$ds^2 = -(1 + 2\frac{\phi}{c^2})c^2 dt^2 + (1 - 2\frac{\phi}{c^2})d\chi^2 + \chi^2 d\Omega^2, \quad (1)$$

where ϕ is the gravitational potential induced by the presence of a single gravitational source. In the presence of multiple sources, we note that this procedure can be used to calculate the time delay for each source individually and then the effects can be summed, since the fields are weak.

We choose a radial null geodesic along the l.o.s. from the emitting source to the observer, working in coordinate time, and find that the total l.t.t. is

$$t = t_0 + \Delta t = \int_{\text{emit}}^{\text{observe}} dt = \int_{\text{emit}}^{\text{observe}} \frac{1}{c} (1 - 2\frac{\phi}{c^2}) d\chi. \quad (2)$$

The first term on the right-hand-side of equation (2) integrates to give a constant (l/c) which we identify as t_0 , or the l.t.t. in the absence of any gravitational sources. The second term is indicative of the time delay (Δt) due to the presence of a gravitational source.

Since the gravitational fields of interest are weak ($\phi/c^2 \ll 1$), it is an excellent approximation to treat ϕ as a Newtonian potential when outside the gravitational source, $\phi = -GM/r$. When one is inside a spherical gravitational source, one must be a little more careful and perform the following integral:

$$\phi = - \int_0^r d^3 r' \frac{G \rho(r')}{r} - \int_r^{r_{\max}} d^3 r' \frac{G \rho(r')}{r'}, \quad (3)$$

which reduces to $\phi = -GM/r$ at $r = r_{\max}$. In general, the effect of the time delay can then be quantified by the integral from the emitter to the observer

$$\Delta t = \int_0^l \frac{-2\phi(x')}{c^3} dx', \quad (4)$$

where the r from equation (3) is the distance between each given position along the l.o.s. (x') and the center-of-mass of the gravitational source. For points lying outside of the source, the total mass (M_{tot}) of the source contributes to ϕ , whereas the gravitational potential can either increase or decrease as one penetrates the source, dependent upon the density profile.

For an extended source of radius r_{\max} , the enclosed mass within the source is given by

$$M_{\text{enc}}(x') = \int_0^{\sqrt{(x' - x_{\parallel})^2 + (x_{\perp})^2}} 4\pi r^2 \rho(r) dr, \quad (5)$$

but merely substituting M_{enc} for M_{tot} is insufficient; one must recalculate ϕ at each point and then solve equation (4). The total mass of the gravitational source (M_{tot}) is given by equation (5) at the point where $r_{\max} = \sqrt{(x' - x_{\parallel})^2 + (x_{\perp})^2}$. In general, therefore, the Shapiro time delay will be given by the combination of equation (4) with the appropriate value for ϕ at all points.

We first consider the case of impact parameters, b , that are larger than the maximal radius (r_{\max}) of the gravitational source in question. This approximation corresponds to the physical cases of baryonic substructures (stars and MA-CHOs) and for non-baryonic substructure where the object is sufficiently far away, even at its point of closest approach, so that its radius never intersects the l.o.s. between the emitter and observer. For this case ($b > r_{\max}$), the enclosed mass is always M_{tot} , and equation (4) is exactly integrable, yielding a time delay of

$$\Delta t = \frac{2GM_{\text{tot}}}{c^3} \ln \left(\frac{l - x_{\parallel} + \sqrt{(l - x_{\parallel})^2 + (x_{\perp})^2}}{-x_{\parallel} + \sqrt{(x_{\parallel})^2 + (x_{\perp})^2}} \right). \quad (6)$$

In the region of physical interest, where the approximation $\{l, x_{\parallel}, l - x_{\parallel}\} \gg \{b, x_{\perp}\}$ is valid, a simpler expression of

$$\Delta t \simeq \frac{2GM_{\text{tot}}}{c^3} \ln \left(\frac{4x_{\parallel}(l - x_{\parallel})}{(x_{\perp})^2} \right) \quad (7)$$

can be obtained. Numerically, this yields a time delay dependent only on the parameters l , \vec{x} , and M_{tot} , such that

$$\Delta t \simeq 2.95 \times 10^{-11} \text{ s} \left(\frac{M_{\text{tot}}}{M_{\oplus}} \right) \ln \left(\frac{4x_{\parallel}(l - x_{\parallel})}{(x_{\perp})^2} \right), \quad (8)$$

where M_{\oplus} is one Earth mass. As the position of the gravitational source, \vec{x} , changes with time, so too will the time delay, Δt . We note that the time delay of equations (6 - 8) depends very weakly on changes in l and x_{\parallel} , but is more sensitive to changes in x_{\perp} , since $x_{\perp} \ll \{x_{\parallel}, l - x_{\parallel}\}$. We also note that these results indicate that the time delay scales linearly with mass, but only logarithmically with position.

As the gravitational sources are expected to be extended objects if they are non-baryonic, we also consider the case that the l.o.s. intersects the gravitational source, so that $b < r_{\max}$. The general equation will still be given by equation (4), although the integration will be significantly more difficult here. Generically, the integral must be broken up into three parts: from the observer to the near edge of the source, from the near edge through the source to the far edge, and from the edge of the source to the emitter. The integral of equation (4) then becomes

$$\begin{aligned} \Delta t &= \int_0^{x_{\parallel} - \sqrt{(r_{\max})^2 - (x_{\perp})^2}} \left(\frac{2GM_{\text{tot}}}{c^3 r} \right) dx' \\ &+ \int_{x_{\parallel} - \sqrt{(r_{\max})^2 - (x_{\perp})^2}}^{x_{\parallel} + \sqrt{(r_{\max})^2 - (x_{\perp})^2}} \left(\frac{-2\phi(x')}{c^3} \right) dx' \\ &+ \int_{x_{\parallel} + \sqrt{(r_{\max})^2 - (x_{\perp})^2}}^l \left(\frac{2GM_{\text{tot}}}{c^3 r} \right) dx', \end{aligned} \quad (9)$$

where $\phi(x')$ is given by equation (3), and is valid for any generic density profile $\rho(r)$ for the gravitational source. An oftentimes more useful form for equation (9) is the partially solved equation

$$\begin{aligned} \Delta t &\simeq \frac{2GM_{\text{tot}}}{c^3} \ln \left[\frac{4x_{\parallel}(l - x_{\parallel})(r_{\max} - \sqrt{(r_{\max})^2 - (x_{\perp})^2})}{(x_{\perp})^2(r_{\max} + \sqrt{(r_{\max})^2 - (x_{\perp})^2})} \right] \\ &+ \int_{x_{\parallel} - \sqrt{(r_{\max})^2 - (x_{\perp})^2}}^{x_{\parallel} + \sqrt{(r_{\max})^2 - (x_{\perp})^2}} \frac{-2\phi(r)}{c^3} d^3 r, \end{aligned} \quad (10)$$

which contains the approximations $x_{\perp} \ll \{x_{\parallel}, l - x_{\parallel}\}$, but still admits a generic density profile $\rho(r)$ (implicit in $\phi(r)$). For all physical cases (i.e., $\rho(r)$ is everywhere non-negative), this leads to a smaller time delay compared to the case of a point mass for sufficiently small values of x_{\perp} . Figure 2 illustrates Δt as a function of x_{\perp} for the case of a point source, the case of a constant density halo with $\rho(r) = 3M_{\text{tot}}/4\pi r_{\max}^3$, as well as the case of a halo with an NFW (Navarro, Frenk, & White 1996, 1997) profile with a cutoff at r_{\max} , obeying the formula

$$\rho(r) = \frac{M_{\text{tot}}}{4\pi r(r_0 + r)^2} \left[\ln \left(1 + \frac{r_{\max}}{r_0} \right) - \frac{r_{\max}}{r_0 + r_{\max}} \right], \quad (11)$$

where r_0 is the turnover radius between an outer halo density falling off as $1/r^3$ and an inner halo density which falls as $1/r$. As can be seen in Figure 2, smaller impact parameters are more sensitive to the form of a gravitational source's density profile.

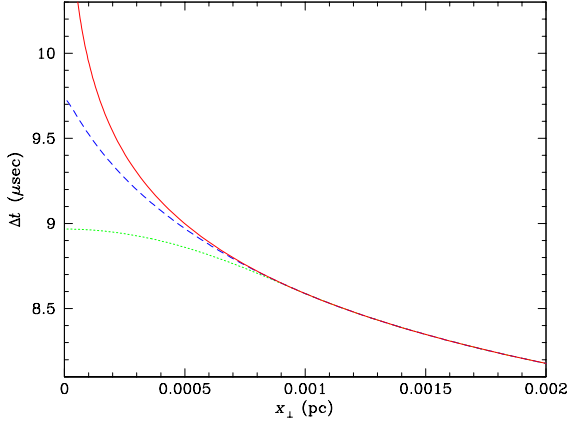


Figure 2. Δt vs. x_{\perp} with $l = 2$ kpc, $x_{\parallel} = 1$ kpc and $M_{\text{tot}} = 10^4 M_{\oplus}$ for three sources: a point source (solid line), a constant density halo (dotted line), and an NFW profile (dashed line). Additionally, the physical size of the gravitational source for extended objects, r_{max} , is chosen to be 10^{-3} pc. The NFW profile illustrated has a turnover radius $r_0 \simeq 10^{-4.5}$ pc. x_{\perp} is plotted in units of parsecs, Δt in units of seconds. This result scales linearly with mass, as indicated in equation (8), so that a microhalo 100 times as massive would have a change in time delay 100 times as large.

3 DARK MATTER DETECTION

The analysis in Section 2 has demonstrated that a gravitational source lying near the l.o.s. between an emission source and an observer will cause a delay in the l.t.t. of the emitted signal. We now specifically turn to the case of our own galaxy for a physical application. It is not possible to measure the absolute l.t.t. of any astrophysical object directly, but *changes* in the l.t.t. can be observed over time. To measure a change in the l.t.t., we require a stable, predictable emitter whose emission properties remain consistent over long timescales. The most stable, consistent emitters in the known universe are the millisecond pulsars, many of which have remained stable without glitches, starquakes, or flux unpinning over timescales exceeding thirty years. Pulsars have been used in many instances in the past to glean information about the physical universe (Detweiler 1979). By treating millisecond pulsars as emission sources, the l.t.t. of each pulse as it heads towards Earth will be quite sensitive to any changes in the matter distribution near the l.o.s. Thus, sufficiently accurate measurements of the l.t.t. will allow us to search for all massive transiting objects near the l.o.s., including MACHOs, WIMPs, and NACHOs.

Pulsars are the ideal candidates to serve as emission sources, as they are the most perfect natural clocks in the known universe. Pulsars exist with a wide variety of rotational periods and also in the emission periods of their pulses. The pulsars with the highest rotational frequencies, and hence the shortest pulse-to-pulse periods, also happen to be the most stable types of pulsars, with a period (T_p) of $\mathcal{O}(1$ ms). These millisecond pulsars have typical residuals of $\mathcal{O}(1 \mu\text{s})$, meaning that if one measures enough pulses accurately (typically over ~ 1 hr timescales), the deviation

of any pulse-to-pulse measurement from the average value is $\mathcal{O}(1 \mu\text{s})$. Remarkably, these residual uncertainties are *not cumulative*, so that the arrival-time uncertainty between the first pulse and the n -th pulse remains $\mathcal{O}(1 \mu\text{s})$, and does not increase as the number of pulses increases. Because of these properties of millisecond pulsars, the ones which are completely stable (no glitches, starquakes, or flux unpinning) have their periods known to an accuracy of $\sim 10^{-17}$ s or better, as an $\mathcal{O}(1 \mu\text{s})$ uncertainty over a span of $\mathcal{O}(10^{12})$ pulses (the first millisecond pulsar was discovered in 1982) yields a measured period accurate to $\sim 10^{-18}$ s.

In order to detect the time delay induced by transiting substructure, the effect must, in some sense, be large when compared with the intrinsic timing uncertainties. The uncertainty in the pulse arrival time is primarily due to environmental uncertainties, owing to the difficulty in modelling both our own and the pulsar’s local environments. In principle, the simplest method for detecting substructure gravitationally would be to determine the shift in the expected pulse arrival time (ΔT_p) for adjacent pulses due to changes in the gravitational potential near the l.o.s. This can be computed by examining the shift in Δt over the time of one pulse, T_p , as the intervening matter changes position. Assuming a constant velocity for the intervening gravitational source, ΔT_p is calculable in general from equation (10) by taking the difference in Δt between an initial source position $\vec{x}_i = (b, x_{\parallel}, x_{\perp})$ and a final source position $\vec{x}_f = (b, x_{\parallel} + v_{\parallel} T_p, x_{\perp} + v_{\perp} T_p)$. So long as ΔT_p is greater than the known period accuracy ($\sim 10^{-17}$ s), it may be possible to extract the signal that would be caused by transiting substructure using statistical techniques, despite the large pulse-to-pulse residuals. ΔT_p as a function of time is shown in Figure 3 for the three transiting cases of a point mass, a constant density extended object, and an extended microhalo with an NFW profile. Unfortunately, this method is not presently feasible in practice for the detection of masses significantly below $1 M_{\odot}$, since pulse arrival times have not been measured to accuracies even approaching 10^{-17} s.

A more complicated, but perhaps more feasible method would be to integrate the observed and expected time delays over many pulses. For this method, we are not constrained by the timescale T_p , as we are free to measure ΔT_p over any time interval that is a multiple of T_p . This allows us to enhance the magnitude of the signal from the pulse-to-pulse values of Figure 3 up to the difference in the time delay between two given positions. The method of computing the change in the l.t.t. is the same as above, except T_p in the final position is to be replaced by nT_p , where n is any positive integer. While the noise residual does not decrease for this case as more pulses are observed, it does not increase either, as the $\mathcal{O}(1 \mu\text{s})$ uncertainty is a non-cumulative error. Therefore, as long as the change in the time delay over a reasonably measurable timescale is comparable to or greater than the residual uncertainties, this signal will be detectable *in practice*. Calculations for the integrated effect of the time delay over many years for a transiting point mass, extended constant density halo, and an extended halo with an NFW profile are illustrated in Figure 4. Quantitatively, for a residual of $\mathcal{O}(1 \mu\text{s})$, a transiting mass of $M_{\text{tot}} \approx 10^4 M_{\oplus}$ with an impact parameter of $b \approx 10^{-4}$ pc will be at the limit of detectability. Detection is made more difficult by the fact that modern pulsar analysis techniques require the removal of lin-

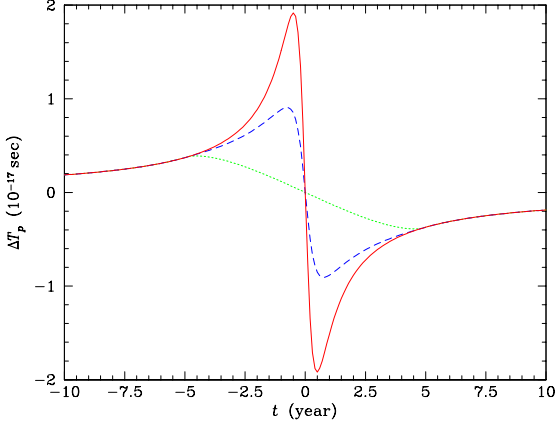


Figure 3. ΔT_p vs. time for a set of parameters corresponding to the variables defined in Figure 2: $l = 2$ kpc, $x_{\parallel} = 1$ kpc, $M_{\text{tot}} = 10^4 M_{\oplus}$, $b = 10^{-4}$ pc, $v_{\perp} = 200$ km s $^{-1}$, and $T_p = 10^{-3}$ s. ΔT_p is illustrated in seconds and time in years. The solid curve is for a point mass, the dotted curve is for a microhalo of constant density with size $r_{\text{max}} = 10^{-3}$ pc, and the dashed curve is for an extended microhalo with an NFW profile of size $r_{\text{max}} = 10^{-3}$ pc and turnover radius $r_0 = 10^{-4.5}$ pc.

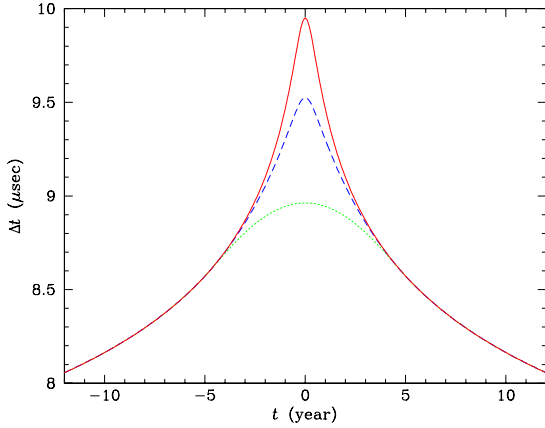


Figure 4. Δt vs. time for a set of parameters corresponding to the variables defined in Figure 2: $l = 2$ kpc, $x_{\parallel} = 1$ kpc, $M_{\text{tot}} = 10^4 M_{\oplus}$, $b = 10^{-4}$ pc, $v_{\perp} = 200$ km s $^{-1}$, and $T_p = 10^{-3}$ s. ΔT_p is illustrated in seconds and time in years. The solid curve is for a point mass, the dotted curve is for a microhalo of constant density with size $r_{\text{max}} = 10^{-3}$ pc, and the dashed curve is for an extended microhalo with an NFW profile of size $r_{\text{max}} = 10^{-3}$ pc and turnover radius $r_0 = 10^{-4.5}$ pc. The chosen set of parameters is very optimistic, but demonstrates the potential power of this method.

ear and quadratic terms from millisecond pulsar data before any further analysis is done. The majority of close dark matter encounters (excepting actual observed transits) will have their signatures absorbed in this subtraction. We suggest, therefore, that it may be beneficial to develop non-standard analysis techniques to explicitly search for this effect.

As can be seen from Figures 3 and 4, the time delay signal is very sensitive to the density profile of the transiting source, and can be used to determine the densities of sufficiently massive transiting dark matter, if their impact parameters are small enough. Halos with steeper density profiles and smaller cores are more easily detectable, whereas the more diffuse ones will have a more significant departure from the point-source template. Of course, at sufficiently large impact parameters, all source behave as point sources. Many of the data analysis techniques being pioneered by groups searching for a cosmic gravitational wave background with pulsars (Jenet et al. 2006) should be applicable to identifying the time delay signature of transiting dark matter substructure. As a caveat, it is worth pointing out that unless the cusp of the Shapiro delay is clearly visible in the residuals, the fit is likely to become degenerate in the presence of noise, as fast-transiting small masses with large impact parameters will be difficult to discern from slow-moving massive objects with small impact parameters.

4 DARK MATTER DISCRIMINATION

The small-scale structure produced in our universe is very sensitive to the type (thermal, non-thermal, or baryonic) and particle properties (masses and couplings) of dark matter. While baryons cannot be all of the dark matter, they do compose a significant amount of the nonluminous matter in the universe (~ 13 per cent). Baryons do not exist in isolation in small mass clumps, but rather as a part of very large mass structures, due to the fact that their collapse is suppressed on all scales which enter the horizon prior to baryon-photon decoupling (at recombination). Therefore, even though baryons exist in the form of diffuse gas clouds and compact halo objects today (in addition to stars), these baryons were never isolated from the non-baryonic dark matter halos in which they are found. The signature that baryonic dark matter (MACHOs) will leave in the pulsar timing measurements is that of a point mass source, as given by changes over time in equation (8). For negligible changes in l and x_{\parallel} , this would result in a pulse-arrival-time shift of

$$\Delta t_f - \Delta t_i \simeq 2.95 \times 10^{-11} \text{ s} \left(\frac{M_{\text{tot}}}{M_{\oplus}} \right) \ln \left(\frac{b^2 + x_z^2}{b^2 + (x_z + v_{\perp} n T_p)^2} \right) \quad (12)$$

between n pulses. Additionally, MACHOs are compact enough that effects such as gravitational microlensing ought to be observable if one knows where to look as well, allowing for possible cross-correlation effects.

The vast majority (~ 87 per cent) of dark matter is non-baryonic, however (contained in Ω_{DM}). In contrast to baryons, the non-baryonic matter is practically collisionless, and thus collapses to form much more diffuse structures than ordinary matter. Additionally, the suppression of non-baryonic structure ceases at a much earlier epoch, as thermal dark matter kinetically decouples from the primordial plasma at a typical temperature of $\mathcal{O}(10 \text{ MeV})$, and non-thermal dark matter is always decoupled both thermally and kinetically from the plasma. The exact epoch of kinetic decoupling of thermally produced dark matter is determined by the mass of the decoupled particles and its interactions; this in turn determines the mass function of small-scale dark matter clumps (Bertschinger 2006). As a result, thermally

produced dark matter will have a sharp drop in its mass function for masses below $\sim 20 M_{\oplus}$, with the exact value dependent upon the exact particle properties chosen. Non-thermal dark matter, by contrast, will not only have no such feature, but may also have a sharp enhancement in the number density of collapsed structures on very small scales under the right conditions. For the case of non-thermally produced axions where the Peccei-Quinn symmetry is broken subsequent to the end of inflation, the initial density fluctuations on scales corresponding to the horizon at $T \simeq \Lambda_{\text{QCD}}$ will be greatly enhanced (Sikivie 2006). This will result in much more numerous and denser structures on these small scales ($M \sim 10^{-6} M_{\oplus}$) as compared with thermal dark matter, although they are still quite diffuse as compared to baryons. While mass scales of $10^{-6} M_{\oplus}$ are far beyond the reach of any foreseeable technology using pulsar timing, this density enhancement will affect larger mass scales as well, and may be detectable if there is a substantial enhancement at mass scales which can be probed, either today or in the future, by pulsar timing.

The surefire way to distinguish between the various types of dark matter is to probe the low end of the mass function, where WIMPs and NACHOs differ from one another in their abundances. Thermal relic dark matter begins to experience a sharp dropoff in the number of collapsed structures at masses below $\sim 20 M_{\oplus}$, although that number is model dependent. If the abundances of these dark matter microhalos can be measured with sufficient accuracy at small mass scales, it may be possible to reconstruct the low end of the mass function, thus constraining the types and properties of dark matter. It is also of interest to probe the density profiles of these structures, which may shed light on not only whether axion miniclusters are present in the universe, but also on the nonlinear collapse of small-scale structure.

In order to calculate the types of observations necessary to probe the effect of transiting dark matter, we must calculate the expected transit rate of these dark microhalos. Moreover, as it is the mass function we desire to probe, different halo masses must be considered and searched for. Press-Schechter theory (Press & Schechter 1974) indicates that the number density of collapsed structures which should be found in our universe today is strongly dependent upon the mass of the structure of interest. At small scales, the mass function is more accurate if replaced by the Sheth-Tormen function (Sheth & Tormen 1999). The mass function dn/dM then obeys the equation

$$\frac{M}{\rho_m} \frac{dn}{d \ln M} = \frac{d(\ln \nu)}{d(\ln M)} \nu f(\nu), \quad (13)$$

with

$$\nu f(\nu) = 0.322 \left[1 + \left(\frac{\nu^2}{\sqrt{2}} \right)^{-0.3} \right] \sqrt{\frac{\sqrt{2}\nu^2}{\pi}} e^{-\frac{\nu^2}{2\sqrt{2}}}, \quad (14)$$

where $\nu = \sigma/\delta_c$, $\delta_c \simeq 1.686$, and σ is the root-mean-squared mass density perturbation in a given region of space. The mass density perturbation spectrum is highly dependent upon the transfer function and power spectrum of the dark matter, and to a lesser extent, the window function. It is estimated in Loeb & Zaldarriaga (2005) that there should be a significant fraction of the Milky Way halo in dark mat-

ter clumps of approximately $10^2 M_{\oplus}$, implying that there are 10^{14} to 10^{15} of these clumps in our galaxy. (A more accurate estimate of the mass function, although it assumes a specific model of thermal dark matter, can be found in Bertschinger (2006).) Assuming a pulsar-to-observer distance of 2 kpc, a typical transverse velocity of a dark matter microhalo of $v_{\perp} \simeq 200 \text{ km s}^{-1}$, 10^{15} microhalos of mass $10^2 M_{\oplus}$, and an NFW profile for the dark matter structure in our own galaxy with a turnover radius of 25 kpc, the local number density of dark matter microhalos is

$$n_{\mu\text{H}} = \frac{\rho_{\mu\text{H}}}{10^{-4} M_{\odot}} \simeq 133 \text{ pc}^{-3}, \quad (15)$$

based on a $\rho(r)$ for the Milky Way given by equation (11) with $r_{\text{max}} = 25r_0$ and our radius from the center of the galaxy taken to be 8 kpc. We note that this estimate is at the high end of the possible number density of microhalos, differing by as much as a factor of $\mathcal{O}(10^2)$ from other estimates. This results in a transit rate near the line-of-sight to a pulsar of

$$\Gamma \sim n_{\mu\text{H}} \sigma v_{\perp} = 0.034 \left(\frac{n_{\mu\text{H}}}{133 \text{ pc}^{-3}} \right) \left(\frac{b_{\text{max}}}{10^{-4} \text{ pc}} \right) \left(\frac{l}{2 \text{ kpc}} \right) \times \left(\frac{v_{\perp}}{200 \text{ km s}^{-1}} \right) \frac{\text{transits}}{\text{year}}, \quad (16)$$

where b_{max} is the maximum impact parameter a microhalo can have relative to the line-of-sight and still be of interest on our observable (~ 25 years) timescales. This rate corresponds to approximately one microhalo with the above properties transiting over the observed timescale of the pulsar. The transit rates for different mass scales and number densities can be computed in a similar fashion for differing mass functions.

The estimates given here are for dark matter microhalos embedded in the galactic halo. The presence of collapsed baryonic substructure, however, particularly in the galactic disk, may alter this profoundly. Extended, low density astrophysical objects such as dark matter microhalos may be gravitationally disrupted (or even captured) by much more dense, massive baryonic structure in the disk as the low density objects pass through (Goerdt et al. 2006). On the other hand, this may not be the case, as globular clusters, which are somewhat more extended and significantly more massive, can remain intact and appear to be undisturbed by the galactic disk (Kobulnicky et al. 2005). It is thus unknown whether dark matter substructure will survive intact in the galactic disk. There may therefore be a tremendous amount of information obtainable by comparing the time-delay effects for pulsars found in the galactic halo, where dark matter substructure may be relatively undisturbed, with those found in the galactic plane.

The net signal which ought to be searched for in the pulsar data is a superposition of all the baryonic MACHOs and dark matter microhalos which transit a significant distance in the x_{\perp} direction with small impact parameters relative to the l.o.s. of the pulsar of interest. Based on the transit rate for low-mass dark matter microhalos computed in equation (16), it ought to be a rare event to observe a transit with a large enough mass ($\sim 10^4 M_{\oplus}$) to be detectable. With $\mathcal{O}(10)$ presently observed pulsars which are sufficiently stable over their observed timescales of $\mathcal{O}(10 \text{ years})$, there is a small but reasonable probability that evidence for dark matter micro-

halos exists in the current pulsar data. Although there are over 100 millisecond pulsars presently known, many of them are either weak radio sources or located in globular clusters, rendering them incapable of detecting dark matter through precision timing campaigns with current instrumentation. The transit rates are small enough so that spatial averaging is not necessary, as only a small number of these dark matter MACHOs (which behave as point sources) and microhalos (which behave as extended sources) of sufficient mass should be observable at all.

5 DISCUSSION

This paper has demonstrated the feasibility of using millisecond pulsars to detect dark matter within our own galaxy. Although the dark matter is distributed in a smooth halo around our galaxy to a zeroth approximation, departures from a smooth density distribution (i.e., clumpiness, cuspy-ness, and caustics) are features of realistic models of dark matter. The dark matter substructure found within our galaxy can be quantified through theoretical modelling of small-scale structure through the deeply nonlinear regime, but can also be probed experimentally through precision measurements of pulsar timing. As the dark matter distribution along the line-of-sight to a pulsar changes over time, the light-travel-time changes as well (as given by equation (4) for an individual source). This effect can be quantified for each source, its effect on the pulse arrival time can be calculated as detailed in Section 3, and summed over all relevant transiting sources. We have illustrated that the rate of interesting events is non-negligible, and such a signal may already be present in archival data. A successful detection of dark matter substructure using pulsar timing would be the first definitive detection of dark matter within our own galaxy.

Beyond merely detecting dark matter substructure, pulsar timing has the potential to provide information about the masses and density profiles of dark matter substructure. Probing galactic substructure is the only method at present capable of measuring the mass function on scales below $\sim 10^6 M_\odot$. Accurate measurements of the mass function on small scales can provide insights into dark matter particle properties such as the type of dark matter (WIMPs or NACHOs), the temperature of kinetic decoupling, and the dark matter's mass and scattering cross sections. Additionally, accurate measurements of the density profile of these dark matter substructures, which is directly related to the time delay signal to be probed by pulsar timing, provides insights into both the particle properties and the nonlinear evolution of dark matter. The density profiles may be significantly different than standard cold dark matter simulations indicate due to dark matter substructures interacting with one another and with baryons, and due to the process of tidal stripping, as analyzed in (Goerdt et al. 2006). While the survivability of these structures is still under debate, it appears to be more of a quantitative question (i.e., what are the percent of surviving halos, what percent are disturbed and to what level, how much of the denser cores survive) than a qualitative one. If strong limits can be placed on the presence of dark matter substructure in the galactic plane

from pulsar timing, it may be evidence indicating that tidal disruption of these small-scale structures is very efficient.

In addition to the effects due to intervening dark matter, there are two other interesting physical phenomena which can interfere with this signal. A gravitational wave background Jenet et al. (2006) is expected to have individual waves containing important effects at the time delay level of $\mathcal{O}(1 \text{ ns})$, with the overall stochastic background contributing a cumulative effect of $\mathcal{O}(100 \text{ ns})$. Although the signal has specific templates which are quite different from that of transiting dark matter, the pulse delay is of the same magnitude for $\mathcal{O}(10^3 M_\oplus)$ substructure as it is for a gravitational wave background, thus care must be taken to distinguish these signals. Additionally, there are baryons in the interstellar medium that can alter the pulse arrival time (Weisberg & Stanimirovic 2007), although their effects may be correctable (You et al. 2007). Although these signals are well-studied, they are anticipated to have significantly larger effects on the pulse arrival time, and thus they must be understood with great care in order to be properly subtracted out.

The possibility of detecting dark matter using pulsar timing is exciting and quite realistic. With the transit rate given in equation (16) and the fact that there are ~ 10 pulsars with the necessary properties for detection, the limiting factor is only to understand the pulsars' timing residuals. Recent advances have allowed pulse-to-pulse residuals for some pulsars to be constrained to $\mathcal{O}(0.1 \mu\text{s})$ with \sim hour-long integration times (van Straten et al. 2001; Jacoby et al. 2005), corresponding to an improved dark matter mass detectability limit of $\sim 10^3 M_\oplus$ for these pulsars. There is an exciting possibility (Edwards, Hobbs, & Manchester 2006) that pulsar timing may soon be accurate to the $\mathcal{O}(1 \text{ ns})$ level, as the software is no longer a barrier to such accuracy. Significant improvements in measurement sensitivity would need to be made as well, of course, but if that happens, it would allow for the detectability of $\sim 10 M_\oplus$ objects, probing past the expected cutoff in the mass function for WIMP dark matter. Although it is estimated in Edwards, Hobbs, & Manchester (2006) that a factor of 10^3 improvement is needed in sensitivity to obtain timing accuracies of $\sim 1 \text{ ns}$, the upcoming Square Kilometer Array will have the sensitivity necessary to improve the residuals by up to two orders of magnitude for many tens of pulsars. It is not, therefore, overly optimistic to consider the method of pulsar timing as having the potential to detect dark matter. We also point out that the use of averaging techniques may allow for a reduction in random errors in the pulsar residuals. When the Square Kilometer Array is complete, and routinely timing hundreds of pulsars to sub- μs accuracy, it is possible that the presence of dark matter clumps may limit the achievable accuracy of pulsar timing, dependent upon the masses and number densities of the dark matter clumps.

An accurate mass function can be derived from Press-Schechter and/or Sheth-Tormen theory via equations (13,14) and the linear power spectrum and transfer function, which can be obtained for any given model of dark matter. Realistically, the mass function can be probed all the way down to this detectability limit and perhaps further, if superior analysis techniques are developed. We emphasize that probing dark matter substructure within our own

galaxy is the only handle on structure formation at scales below ~ 100 kpc at present. Furthermore, there may also be a correlation between dark matter microhalos that are either sufficiently massive, dense, or nearby and a possible WIMP annihilation signal (de Boer et al. 2005), which may provide further information about the nature of dark matter.

Uncovering the nature of dark matter remains one of the most important problems in cosmology today. Precision pulsar timing measurements can be used to probe dark matter substructure transiting near the line-of-sight within our own galaxy. Changes in the light-travel-time of emitted pulses, although small (of order 10^{-6} s) and over long (~ 10 years) timescales, are nonetheless observable *in practice* based on the current accuracy of pulsar timing. Improvements in the understanding of pulsars themselves, as well as the local environments of the pulsar and our solar system, will allow us to probe smaller and smaller mass scales. Additionally, information gained about the transiting substructure can be used to constrain both the particle properties of dark matter and the density profiles of that structure. Overall, pulsar timing measurements may provide a new window into uncovering the properties, method of creation, and evolution of the non-luminous matter in our universe.

ACKNOWLEDGMENTS

We acknowledge the Les Houches Summer School for hospitality and thank the Dark Matter Working Group and Edoardo Di Napoli in particular for extremely helpful conversations during the formative stages of this work. We also acknowledge Kathryn Zurek, and Konstantin Borozdin for useful discussions. E.R.S. thanks the University of Wisconsin for support during the completion of this work. M. P. H. is supported in part by funds provided by the U.S. Department of Energy (D.O.E.) under cooperative research agreement DE-FG02-05ER41360.

REFERENCES

- Alcock C. et al. [MACHO Collaboration], 1998, ApJ, 499, L9
- Baez J.C., Bunn, E.F., 2005, AJP, 73, 644
- Bertschinger E., 2006, Phys. Rev. D, 74, 063509
- Clowe D., Bradac M., Gonzalez A.H., Markevitch M., Randall S.W., Jones C., Zaritsky D., arXiv:astro-ph/0608407
- de Boer W., Sander C., Zhukov V., Gladyshev A.V., Kazakov D.I., 2005, Phys. Rev. Lett., 95, 209001
- Detweiler S., 1979, ApJ, 234, 1100
- Diemand J., Moore B., Stadel J., 2005, Nat, 433, 389
- Dubovsky S.L., Tinyakov P.G., Tkachev I.I., 2005, Phys. Rev. Lett., 94, 181102
- Edwards R.T., Hobbs G.B., Manchester, R.N., 2006, MNRAS, 372, 1549
- Fields B.D., Olive K.A., 2006, Nuc. Phys. A, 777, 208
- Fukugita M., Peebles P.J.E., 2004, ApJ, 616, 643
- Goerdt T., Gnedin O.Y., Moore B., Diemand J., Stadel J., arXiv:astro-ph/0608495
- Green A.M., Hofmann S., Schwarz D.J., 2005, JCAP, 0508, 003
- Jacoby B.A., Hotan A., Bailes M., Ord S., Kulkarni S.R., 2005, ApJ, 629, L113
- Jenet F.A. et al., 2006, ApJ, 653, 1571
- Kobulnicky H.A. et al., 2005, AJ, 129, 239
- Loeb A., Zaldarriaga M., 2005, Phys. Rev. D, 71, 103520
- Miller C.J., Nichol R.C., Chen X.L., 2002, ApJ, 579, 483
- Navarro J.F., Frenk C.S., White S.D.M., 1996, ApJ, 462, 563
- Navarro J.F., Frenk C.S., White S.D.M., 1997, ApJ, 490, 493
- Peccei R.D., Quinn H.R., 1977, Phys. Rev. Lett., 38, 1440
- Press W.H., Schechter P., 1974, ApJ, 187, 425
- Riess A.G. et al., arXiv:astro-ph/0611572
- Shankar F., Lapi A., Salucci P., De Zotti G., Danese L., 2006, ApJ, 643, 14
- Shapiro I.I., 1964, Phys. Rev. Lett., 13, 789
- Sheth R.K., Tormen G., 1999, MNRAS, 308, 119
- Siegel E.R. et al., arXiv:astro-ph/0611864
- Sikivie, P., arXiv:astro-ph/0610440
- Spergel D.N. et al., arXiv:astro-ph/0603449
- van Straten W., Bailes M., Britton M., Kulkarni S.R., Anderson S.B., Manchester R.N., Sarkissian J., 2001, Nature, 412, 158
- Viel M., Lesgourgues J., Haehnelt J.G., Matarrese S., Riotto A., 2005, Phys. Rev. D, 71, 063534
- Weinberg S., 1978, Phys. Rev. Lett., 40, 223
- Weisberg J.M., Stanimirovic S., 2007, arXiv:astro-ph/0701771
- Wilczek F., 1978, Phys. Rev. Lett., 40, 279
- You X.P. et al., 2007, arXiv:astro-ph/0702366
- Zurek K.M., Hogan C.J., Quinn T.R., arXiv:astro-ph/0607341